Hindawi Publishing Corporation
Indian Journal of Materials Science
Volume 2013, Article ID 516812, 8 pages
http://dx.doi.org/10.1155/2013/516812

Research Article

Structural, Optical and Electrical Properties of $Sn_xZn_{1-x}O_{1+x}$ Thin Films Using Nebulizer Spray Pyrolysis Technique

R. Mariappan,[1,2] V. Ponnuswamy,[1] P. Jayamurugan,[1,2] R. N. Jayaprakash,[2] and R. Suresh[1]

[1] *Department of Physics, Sri Ramakrishna Mission Vidyalaya College of Arts and Science, Coimbatore, Tamilnadu 641 020, India*
[2] *Department of Physics, Adhiyamaan College of Engineering, Hosur, Tamilnadu 635 109, India*

Correspondence should be addressed to V. Ponnuswamy; mari.tf@rediff.com

Received 16 July 2013; Accepted 16 August 2013

Academic Editors: A. Evteev and V. Privman

$Sn_xZn_{1-x}O_{1+x}$ thin films have been deposited on glass substrates at substrate temperature 400°C through nebulizer spray pyrolysis technique. X-ray diffraction (XRD) analysis shows that the films structure is changed from hexagonal to tetragonal. The high-resolution scanning electron microscopy (HRSEM) studies reveal that the substrate is well covered with a number of grains indicating compact morphology with an average grain size 50–79 nm. Energy dispersive X-ray analysis (EDAX) reveals the average ratio of the atomic percentage. Optical transmittance study shows the presence of direct transition. Band gap energy decreases from 3.33 to 2.87 eV with respect to the rise of Sn content. The electrical resistivity of the thin films was found to be 10^6 Ω-m.

1. Introduction

Recently, the application range of semiconductor gas sensors prepared out of metal oxides such as ZnO, TiO_2, CdO, SnO_2, and In_2O_3 is spreading more to detect the pollutants, toxic gases, alcohol, and food freshness. It is known that the electrical conductivity of semiconductors like ZnO, SnO_2 and CdO increases while they form compounds like Sn substituted CdO and Sn substituted ZnO. These materials find applications in sensing devices like gas sensors, moisture detectors, and electronic sensors [1–4]. At present, research interest has been shifted to thin film sensors [5]. Sn substituted ZnO is sensitive to many gases like hydrocarbons [6], H_2 [7], oxygen [8], and so forth and also has satisfactory stability. Sn substituted ZnO thin films can be prepared by a variety of techniques, such as low-temperature ion exchange method [9], coprecipitation method [2], and thermal evaporation [10]. Nebulizer spray technique is widely used because it is simple and economically viable technique, which produces films of good quality for device applications. The preparation method for sensing material therefore plays an important role in the morphological characteristics and control over the particle size and surface area of the sensor.

In the present work, preparation and characterization of $ZnSnO_3$ thin films by simple and low cost nebulizer spray pyrolysis technique have been reported. The films were characterized by X-ray diffraction (XRD), scanning electron microscopy (SEM), energy dispersive X-ray analysis (EDX), CO gas sensitivity, electrical conductivity, and optical measurements. The results are discussed and reported.

2. Experimental Technique

Chemicals used for the deposition of $Sn_xZn_{1-x}O_{1+x}$ were analytical grade zinc chloride, tin (IV) chloride, sodium hydroxide pallet, ethylene diamine tetraacetic acid salt (EDTA), and deionized water.

$Sn_xZn_{1-x}O_{1+x}$ films were prepared at different temperatures using nebulizer spray pyrolysis (NSP) technique. 0.1 M Zinc chloride was dissolved in 25 mL of de-ionized water and stirred for 10 minutes using magnetic stirrer. NaOH solution was added slowly from a burette held vertically with Zinc chloride solution until the pH value reached 7. Similarly, 0.1 M tin (IV) chloride solution was prepared. 0.02 M of EDTA was added to the above solution, and stirring was continued for 30 min. Tin (IV) chloride solution was added with zinc chloride solution slowly under gentle stirring condition. Then NaOH solution was again added till the pH value reached 7. 50 mL of the prepared solution was sprayed onto glass substrates.

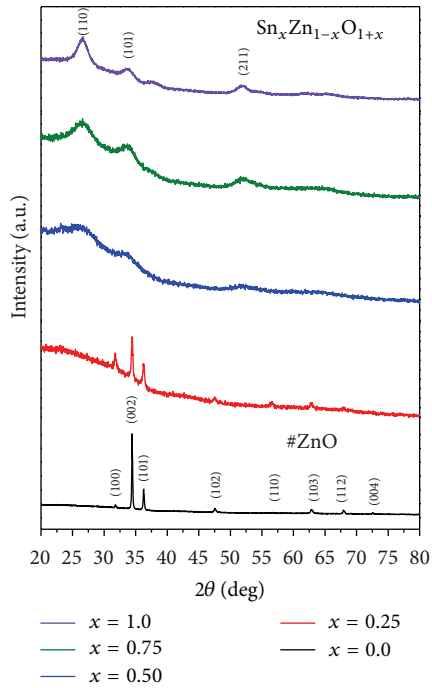

Figure 1: X-ray diffraction patterns of $Sn_xZn_{1-x}O_{1+x}$ thin films.

X-ray diffraction data of the nebulizer sprayed $Sn_xZn_{1-x}O_{1+x}$ films were recorded with the help of Philips Model PW 1710 diffractometer with Cu Kα radiation ($\lambda = 0.1542$ nm). Surface morphological studies and compositional analysis were carried out using a scanning electron microscope and energy dispersive X-ray analysis (EDAX) setup which is attached with SEM (Philips Model XL 30), respectively. Optical absorption spectrum was recorded using a JASCO-V-570 spectrophotometer. The room temperature photoluminescence (PL) spectrum was recorded with spectrofluorimeter (Fluorolog Model FL3-11). The electrical resistivity of the films was studied using a four-probe method.

3. Results and Discussion

3.1. Structural Analysis of $Sn_xZn_{1-x}O_{1+x}$ Thin Films. X-ray diffraction patterns recorded for the $Sn_xZn_{1-x}O_{1+x}$ thin films on glass substrates at 400°C with different compositions (x) are shown in Figure 1. The different peaks in the diffractogram were indexed, and the corresponding values of interplanar spacing "d" were calculated and compared with the standard JCPDS values [11, 12]. The XRD reveals that for $x \leq 0.25$, the crystal structure of $Sn_xZn_{1-x}O_{1+x}$ thin films is hexagonal crystal structure with X-ray diffraction peaks corresponding to [100], [002], [101], [102], [110], [103], [112], and [004] planes. For $x \geq 0.5$, however, the $Sn_xZn_{1-x}O_{1+x}$ thin films were grown with tetragonal structure with the prominent X-Ray diffraction peaks corresponding to [110], [101], and [211] planes. This means that the transition form the hexagonal structure to the tetragonal from takes between $x \leq 0.25$ and $x \geq 0.75$. It is observed that (Figure 1) the diffraction angle [101], shift towards lower scattering angles with an increase in the compositions (x). The lattice constants (a, c) were calculated using (1) and (2) for the $Sn_xZn_{1-x}O_{1+x}$ films as follows:

When $x = 0$ to $x \leq 0.25$,

$$\frac{1}{d^2} = \frac{4}{3}\left[\frac{\left(h^2 + hk + k^2\right)}{a^2}\right] + \frac{l^2}{c^2} \quad (1)$$

and when $x \geq 0.5$,

$$\frac{1}{d^2} = \frac{\left(h^2 + k^2\right)}{a^2} + \frac{l^2}{c^2}. \quad (2)$$

The variations of lattice constants ("a" and "c") with composition (x) of the $Sn_xZn_{1-x}O_{1+x}$ films are shown in Figure 2(a). It is observed that the lattice constant ("a") values of $Sn_xZn_{1-x}O_{1+x}$ thin films are increased with an increase in the compositions (x), while lattice constant ("c") decreases as shown in Figure 2(a). The crystallite size of $Sn_xZn_{1-x}O_{1+x}$ thin films was evaluated using the following Debye-Scherer formula [13]:

$$D = \frac{0.9\lambda}{\beta \cos\theta}, \quad (3)$$

where D is the mean crystallite size, β is the full width at half maximum of the diffraction line, θ is diffraction angle, and λ is the wavelength of the X-radiation. The variations of crystallite size with composition (x) for the $Sn_xZn_{1-x}O_{1+x}$ films are shown in Figure 2(b). From Figure 2(b), it is observed that the crystallite size of the $Sn_xZn_{1-x}O_{1+x}$ films decreases with increase in composition up to $x \leq 0.5$ after slightly increased.

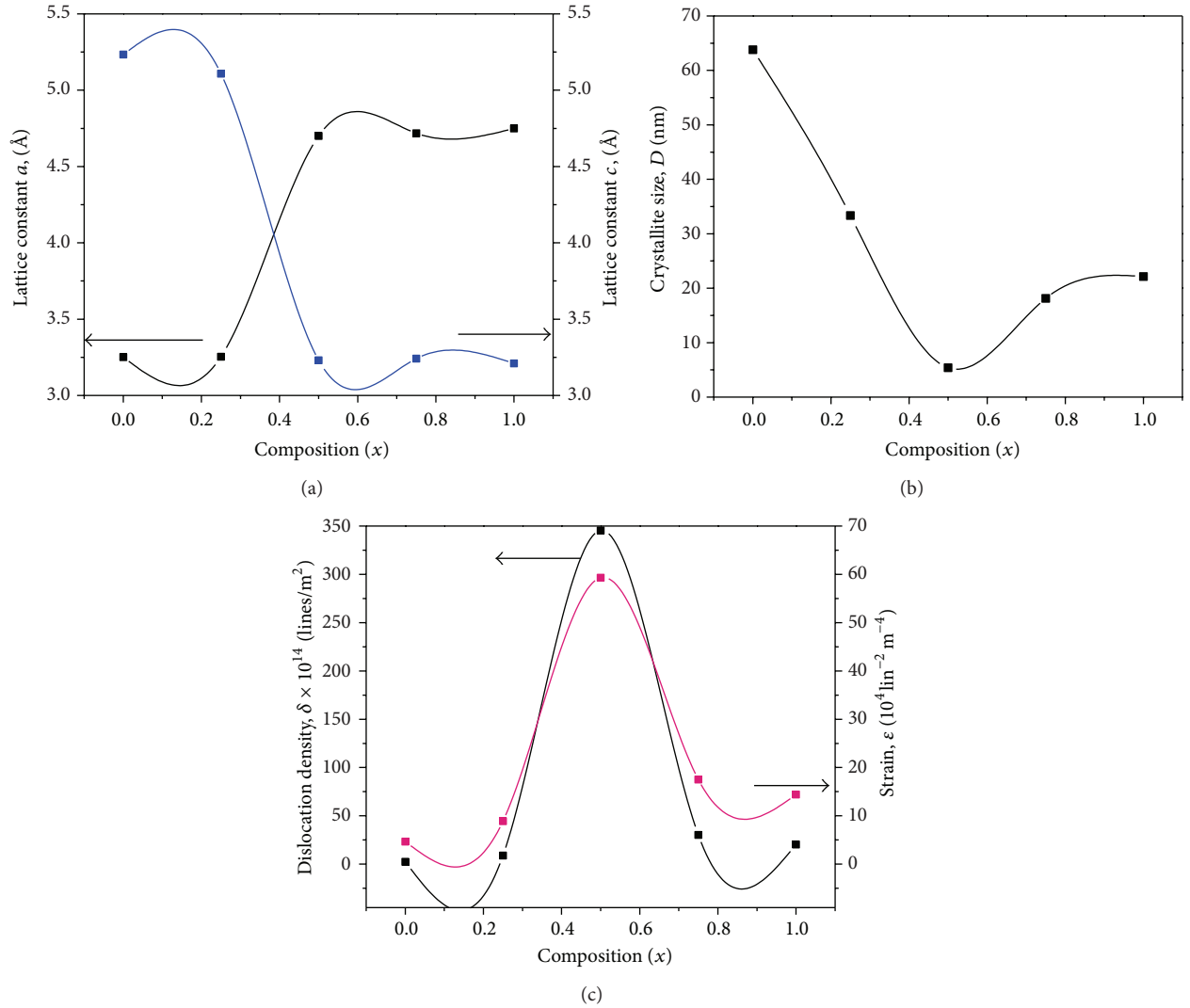

FIGURE 2: Variations of (a) lattice constants (a, c), (b) crystallite size, and (c) dislocation density and strain with composition (x) for the $Sn_xZn_{1-x}O_{1+x}$ thin films.

The dislocation density (δ) and strain (ε) were calculated for the $Sn_xZn_{1-x}O_{1+x}$ thin films using [13]

$$\delta = \frac{1}{D^2}\ \text{lines/m}^2, \qquad \varepsilon = \frac{\lambda}{D\sin\theta} - \frac{\beta}{\tan\theta}. \tag{4}$$

The crystallization levels of the films are good because of their small dislocation density (δ) and lower strain (ε) values which represent the amount of defects in the film. The variations of dislocation density and strain with composition (x) for the $Sn_xZn_{1-x}O_{1+x}$ thin films are shown in Figure 2(c). It is observed that (Figure 2(c)) a sharp decrease in dislocation density and strain of the films and the corresponding minimum values are recorded for composition $x = 1.0$.

3.2. Surface Morphological Studies of $Sn_xZn_{1-x}O_{1+x}$ Thin Films. Figures 3(a)–3(c) show the surface morphology and the different magnification images of $Sn_xZn_{1-x}O_{1+x}$ films grown at 400°C with different compositions $x = 0$, 0.5, and 1, respectively. It is apparent from the electron micrograph that the change in morphology is strongly dependent on the Sn compositions (x) of the films. It is observed that (Figure 3(a)) the granular surface of ZnO film is smooth, dense, without pinholes, and with uniform nanowalls. For the estimation of average grain size of films, a line was drawn on the high-resolution SEM image, and its length was divided by the number of grain boundaries crossing the line. The grains are uniformly distributed with varied thicknesses for the nanowall like structures between 34 and 61 nm for pure ZnO film. The surface morphology of the films is more or less the same and is similar to that of Figure 3(b) as long as the Sn composition ($x = 0.5$), the surface showing smooth and agglomeration of grains without creaks or pinholes and well covered to the glass substrate. As the composition is increased to $x = 1.0$ (Figure 3(c)), small and uniform spherical grains and well-defined grain boundaries are found in the high-resolution SEM images.

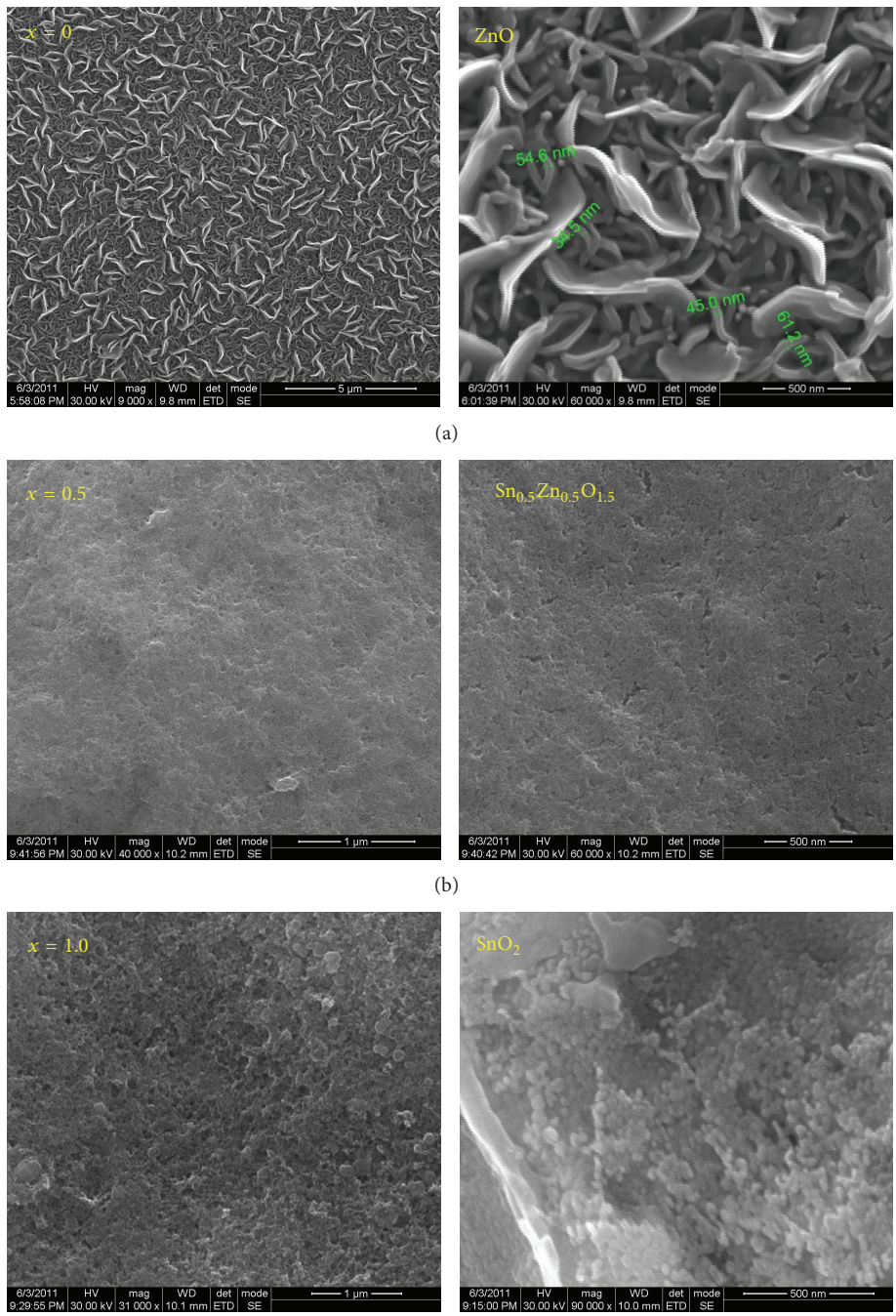

FIGURE 3: High-resolution SEM images of $Sn_xZn_{1-x}O_{1+x}$ thin films with compositions (a) $x = 0$, (b) $x = 0.5$, and $x = 1.0$.

3.3. Commotional Analysis of $Sn_xZn_{1-x}O_{1+x}$ Thin Films. The compositional analysis of the nebulizer-sprayed $Sn_xZn_{1-x}O_{1+x}$ thin films deposited at 400°C with different compositions was done using energy dispersive X-ray analysis (EDAX). The EDAX spectra of $Sn_xZn_{1-x}O_{1+x}$ films deposited at 400°C are shown in Figures 4(a)–4(c). It is observed from Figure 4(a) that the average atomic percentage of Zn : O was 50.14 : 44.49 with nearly better stoichiometry in ZnO film. In $Sn_{0.5}Zn_{0.5}O_{1.5}$ film the average atomic percentage of Sn : Zn : O was 16.94 : 18.81 : 58.98 for $x = 0.5$ (Figure 4(b)). Zn content was replaced by Sn content in $Sn_xZn_{1-x}O_{1+x}$ solid solution films, definitely leading to crystallographic disorder. Sn or Zn interstitial may be created simultaneously. For $x = 1$, in SnO_2 film, the average atomic percentage of Sn : O was 29.43 : 66.32 showing that the samples highly oxygen rich. The EDAX result is consistent with X-ray diffraction analysis of the sample with phase corresponding to ZnO, $Sn_{0.5}Zn_{0.5}O_{1.5}$, and SnO_2. Therefore, the films deposited at 400°C are nearly stoichiometric.

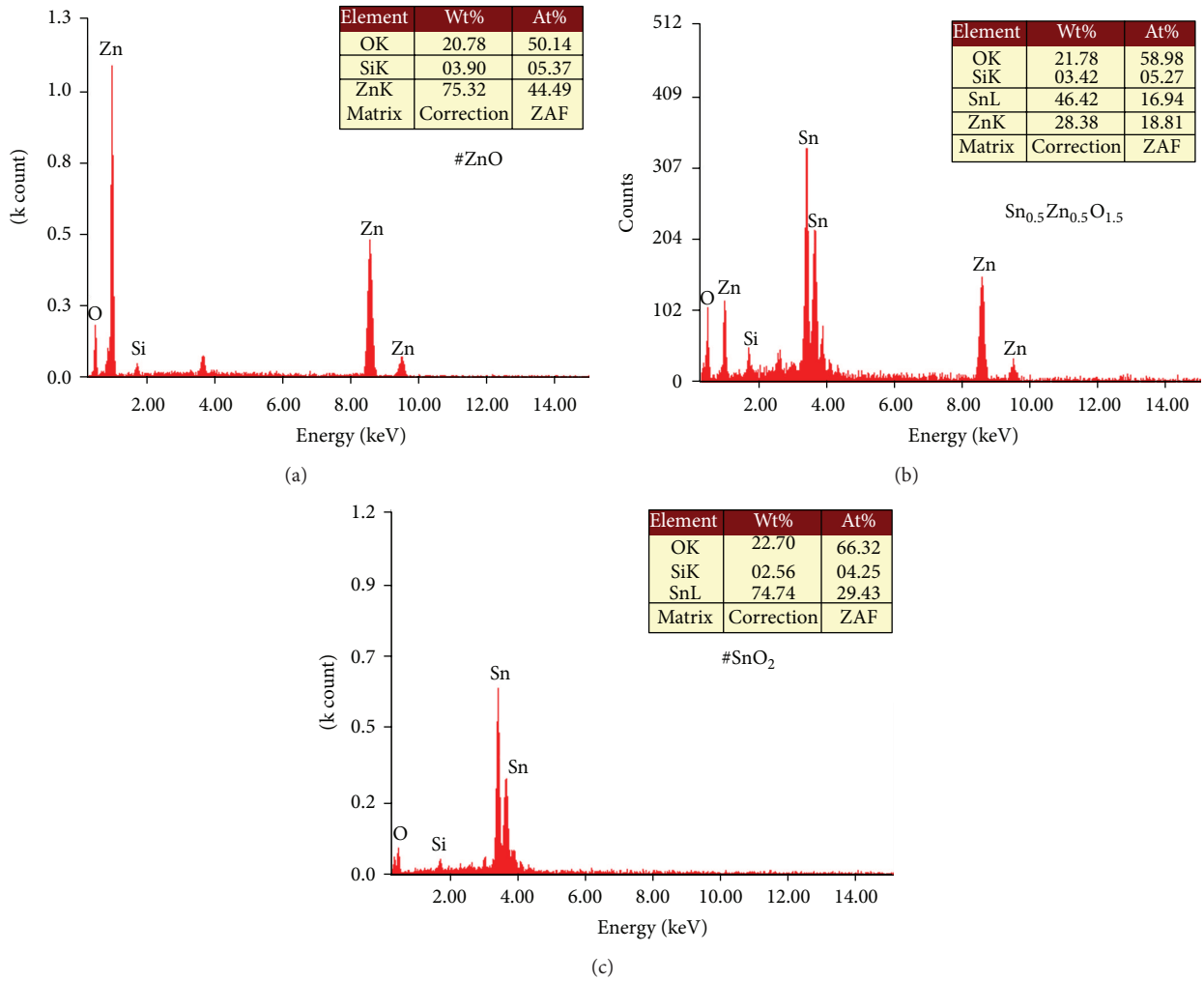

FIGURE 4: EDAX spectra of $Sn_xZn_{1-x}O_{1+x}$ thin films with compositions (a) $x = 0$, (b) $x = 0.5$ and $x = 1.0$.

3.4. Optical Properties of $Sn_xZn_{1-x}O_{1+x}$ Thin Films. Figure 5(a) shows the optical transmission spectra recorded in the range 300–2500 nm of the $Sn_xZn_{1-x}O_{1+x}$ thin films deposited at 400°C with different compositions. The values of the transmission obtained vary from 40% to 85% for the films. The film transparency decreases with the increase of the thickness in all films. In addition, a strong absorption region, which corresponds to the fundamental absorption due to the interband electronic transition, is seen in the higher photon energy region. The band gap energy is calculated by using the following equation:

$$(\alpha h\nu)^n = A\,(h\nu - \mathrm{Eg})\,, \tag{5}$$

where A is a constant, Eg is the band gap energy, and $n = 2$ for direct band gap semiconductors, such as $Sn_xZn_{1-x}O_{1+x}$ films. A plot of $(\alpha h\nu)^2$ versus $(h\nu)$ is a straight line whose intercept on energy axis gives the energy gap "Eg" as shown in Figure 5(b). The optical band gap energy values (Eg) were calculated by plotting the value of $(\alpha h\nu)^2$ against the photon energy $(h\nu)$, and the intercept of this linear region on the energy axis at $(\alpha h\nu)^2$ equal to zero gives the band gap. The band gap energy (Eg) values slightly decrease with the compositions from $x = 0$ to 1.0. The band gap energy values decreases from 3.33 to 2.87 eV, which is compared well with the reported values [14, 15].

3.5. Photoluminescence Studies of $Sn_xZn_{1-x}O_{1+x}$ Thin Films. Photoluminescence emission spectra of $Sn_xZn_{1-x}O_{1+x}$ thin films deposited at 400°C are shown in Figure 6. The spectra have been recorded at room temperature with an excitation wavelength of 378 nm. For $x = 0$, pure ZnO films exhibit three broad emission peaks, called ultraviolet, blue, and green peaks located around 390 nm, 437 nm, and 467 nm, respectively. As the photoluminescence peak energies are less than the energy gap, these bands can be definitely identified with transitions involving donors, acceptors, free electrons, and holes [16]. Thus, the well-known green band can be attributed to the recombination between donor and acceptor levels originated from surface states, that is, grain boundaries, pinholes, microdeformation, adsorbed oxygen, and so forth [16]. In the photoluminescence spectra the peak can be attributed to high concentration of defects. The broadening of the peaks can be ascribed to the fact that large crystals tend

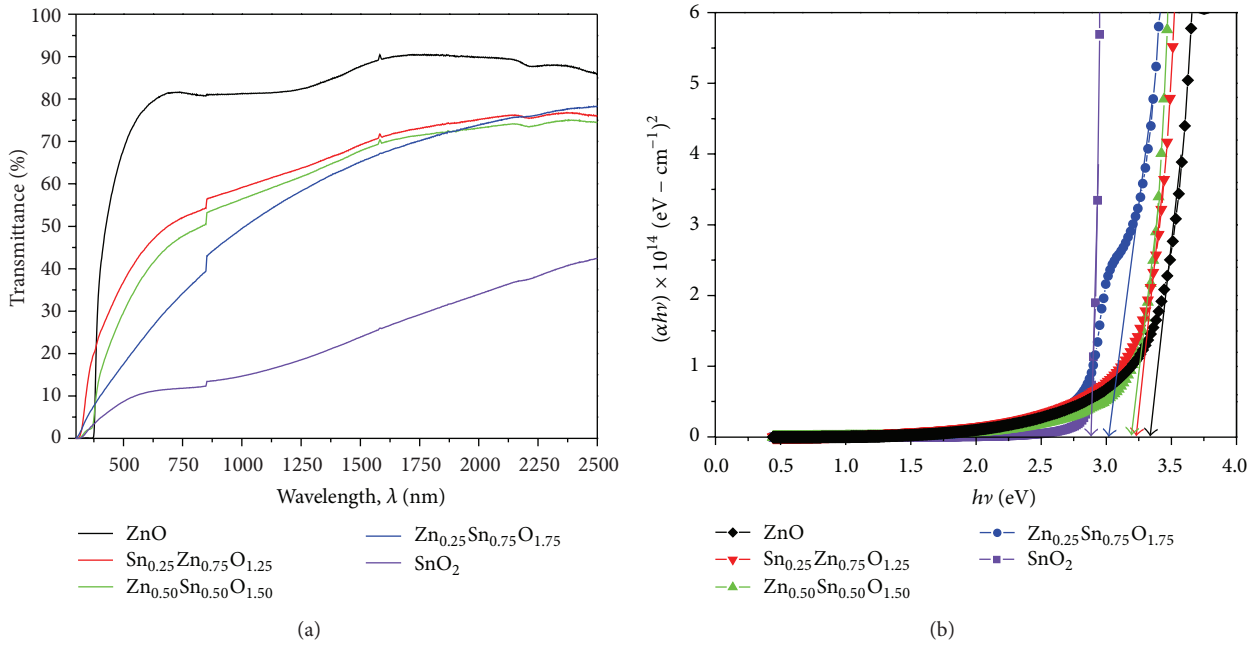

FIGURE 5: (a) Trabsmittance spectra of $Sn_xZn_{1-x}O_{1+x}$ thin films. (b) Plots of $(\alpha h\nu)^2$ versus $(h\nu)$ for the $Sn_xZn_{1-x}O_{1+x}$ thin films.

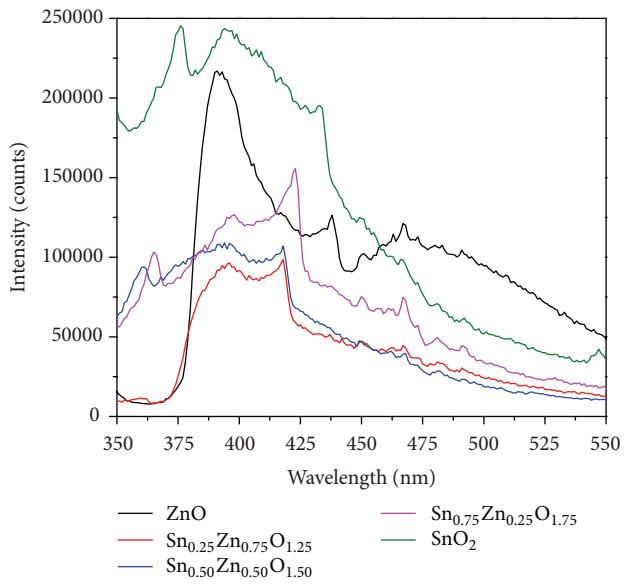

FIGURE 6: Photoluminescence spectra of $Sn_xZn_{1-x}O_{1+x}$ thin films.

to harbor more defects than small crystals. These defects may act as nonradiative recombination centres, which band edge recombination [17]. It is observed that (Figure 6) the emission spectra are also found to decrease in intensity with decrease in grain size due to the increase in composition from $x \geq 2.5$ to $x \leq 7.5$. For $x = 1$, SnO_2 thin films are excited at 361 nm. The plot contains the three peaks centred at 376 nm, 394 nm, and 433 nm. The peak at 433 nm is due to the recombination between the oxygen vacancies related donor and the valence band [18].

3.6. I-V Characteristics of $Sn_xZn_{1-x}O_{1+x}$ Thin Films. The electrical resistivity of the $Sn_xZn_{1-x}O_{1+x}$ thin films is calculated from the following equation

$$\rho = \left(\frac{V}{I}\right) x \left(\frac{A}{l}\right), \tag{6}$$

where V is the applied voltage, I is the current, A is the area of the films, and l is the thickness. In order to investigate the rectifying behavior of the films at different temperatures, I-V characteristics are obtained by connecting Keithley electrometer to the four-probe method. Figures 7(a)–7(c) shows the I-V characteristics of $Sn_xZn_{1-x}O_{1+x}$ thin films deposited at 400°C with different compositions. The resistivity of the $Sn_xZn_{1-x}O_{1+x}$ films decreases with increase in temperature indicating the development of semiconducting nature. It is observed (Figure 7(d)) that the resistivity decreases nonlinearly with the increase of temperature. It is well known that electrical properties of polycrystalline films are strongly influenced by their structural characteristics and nature of purity.

3.7. Conclusion. The $Sn_xZn_{1-x}O_{1+x}$ thin films are potential candidates used in various applications like photovoltaic and optoelectronics devices and gas sensors fabrications. The $Sn_xZn_{1-x}O_{1+x}$ thin films were deposited at 400°C with different compositions (x) through the nebulizer spray pyrolysis technique. X-ray diffraction study shows the formation of polycrystalline $Sn_xZn_{1-x}O_{1+x}$ films with preferential orientation along [002] and [101], shift towards lower scattering angles with an increase in the compositions (x). The structure of the films has been transformed from hexagonal to tetragonal structure. The surface morphology and grain size also change with an increase in the compositions (x)

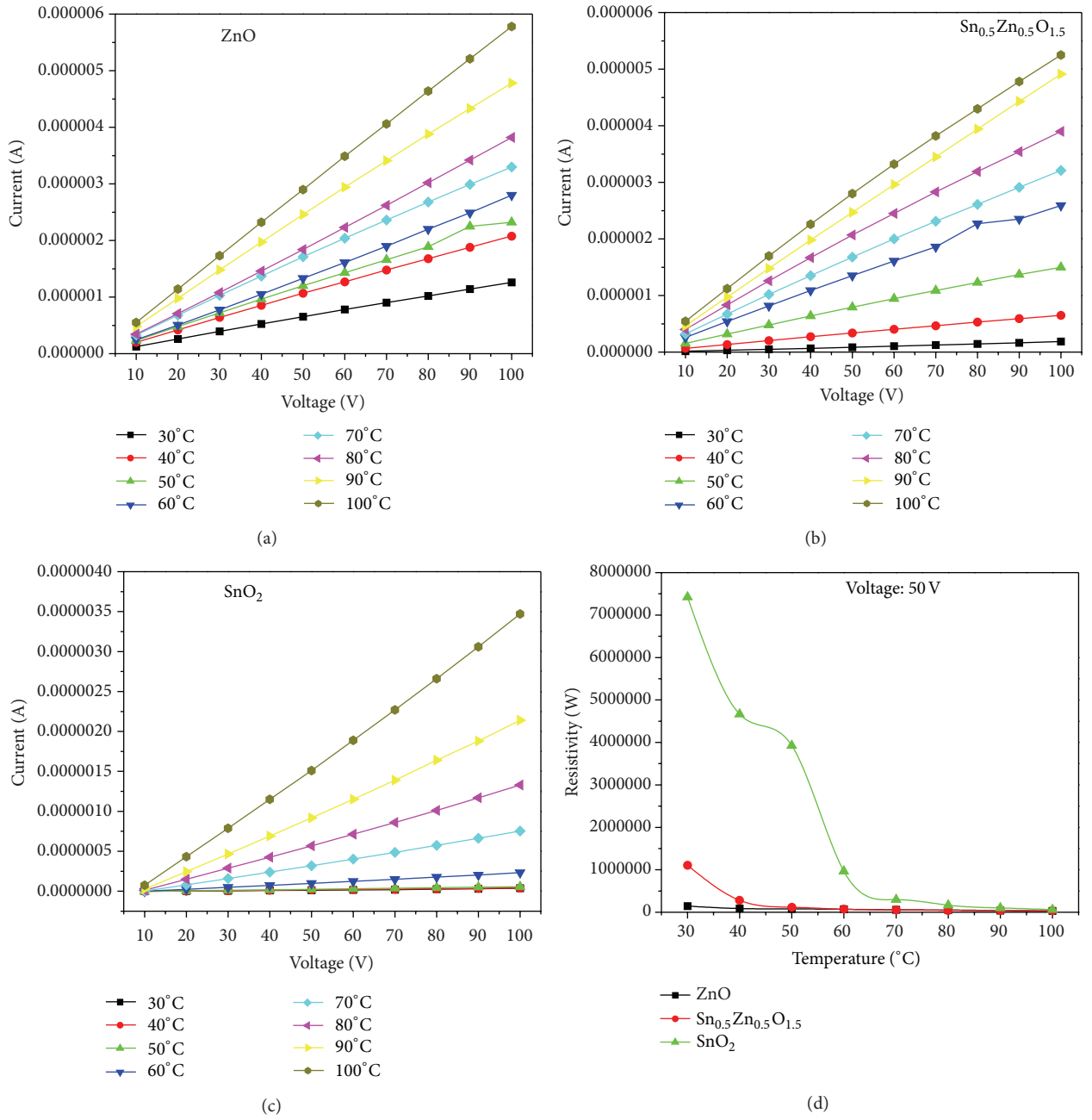

FIGURE 7: *I-V* characteristics of $Sn_xZn_{1-x}O_{1+x}$ thin films with compositions (a) $x = 0$, (b) $x = 0.5$, and (c) $x = 1.0$ and (d) variations of resistivity with temperature for $Sn_xZn_{1-x}O_{1+x}$ thin films.

which has been confirmed from XRD studies. The EDAX result is consistent with energy dispersive X-ray analysis of the films with phase corresponding to ZnO, $Sn_{0.5}Zn_{0.5}O_{1.5}$, and SnO_2. Therefore, the films deposited at 400°C are nearly stoichiometric. The optical studies confirm the decrease of band gap energy with an increase of composition, and the optical band gap energy of the films is found to be decreased from 3.33 to 2.87 eV. The resistivity of the $Sn_xZn_{1-x}O_{1+x}$ films decreases with increase in temperature, while conductivity also increased. It is indicating the development of semiconducting nature of the films. The investigation results of the $Sn_xZn_{1-x}O_{1+x}$ prepared by nebulizer spray films ensure their stability and suitability for optoelectronics devices.

References

[1] S. Yu-Sheng and Z. Tian-Shu, "Preparation, structure and gas-sensing properties of ultramicro $ZnSnO_3$ powder," *Sensors and Actuators B*, vol. 12, no. 1, pp. 5–9, 1993.

[2] T. Zhang, Y. Shen, and R. Zhang, "Ilmenite structure-type β-$CdSnO_3$ used as an ethanol sensing material," *Materials Letters*, vol. 23, no. 1–3, pp. 69–71, 1995.

[3] W. Xing-Hui, W. Yu-De, L. Yan-Feng, and Z. Zhen-Lai, "Electrical and gas-sensing properties of perovskite-type $CdSnO_3$ semiconductor material," *Materials Chemistry and Physics*, vol. 77, no. 2, pp. 588–593, 2003.

[4] X.-H. Wu, Y.-D. Wang, Z.-H. Tian, H.-L. Liu, Z.-L. Zhou, and Y.-F. Li, "Study on $ZnSnO_3$ sensitive material based on combustible gases," *Solid-State Electronics*, vol. 46, no. 5, pp. 715–719, 2002.

[5] V. Demarne and A. Grisel, "An integrated low-power thin-film CO gas sensor on silicon," *Sensors and Actuators*, vol. 13, no. 4, pp. 301–313, 1988.

[6] A. Jones, T. A. Jones, B. Mann, and J. G. Firth, "The effect of the physical form of the oxide on the conductivity changes produced by CH_4, CO and H_2O on ZnO," *Sensors and Actuators*, vol. 5, no. 1, pp. 75–88, 1984.

[7] S. Basu and A. Dutta, "Modified heterojunction based on zinc oxide thin film for hydrogen gas-sensor application," *Sensors and Actuators B*, vol. 22, no. 2, pp. 83–87, 1994.

[8] G. Sberveglieri, P. Nelli, S. Groppelli, F. Quaranta, A. Valentini, and L. Vasanelli, "Oxygen gas sensing characteristics at ambient pressure of undoped and lithium-doped ZnO-sputtered thin films," *Materials Science and Engineering B*, vol. 7, no. 1-2, pp. 63–68, 1990.

[9] D. Kovacheva and K. Petrov, "Preparation of crystalline $ZnSnO_3$ from Li_2SnO_3 by low-temperature ion exchange," *Solid State Ionics*, vol. 109, no. 3-4, pp. 327–332, 1998.

[10] X. Y. Xue, Y. J. Chen, Y. G. Wang, and T. H. Wang, "Synthesis and ethanol sensing properties of $ZnSnO_3$ nanowires," *Applied Physics Letters*, vol. 86, no. 23, Article ID 233101, 3 pages, 2005.

[11] R. B. Heller, J. McGannon, and A. H. Weber, "Precision determination of the lattice constants of zinc oxide," *Journal of Applied Physics*, vol. 21, no. 12, pp. 1283–1284, 1950.

[12] A. A. Bolzan, C. Fong, B. J. Kennedy, and C. J. Howard, "Structural studies of rutile-type metal dioxides," *Acta Crystallographica B*, vol. 53, pp. 373–380, 1997.

[13] R. Mariappan, V. Ponnuswamy, and M. Ragavendar, "Effect of doping concentration on the structural and optical properties of pure and tin doped zinc oxide thin films by nebulizer spray pyrolysis (NSP) technique," *Superlattices and Microstructures*, vol. 52, pp. 500–513, 2012.

[14] M. Hezam, N. Tabet, and A. Mekki, "Synthesis and characterization of DC magnetron sputtered ZnO thin films under high working pressures," *Thin Solid Films*, vol. 518, no. 24, pp. 161–164, 2010.

[15] G. E. Patil, D. D. Kajale, D. N. Chavan et al., "Synthesis, characterization and gas sensing performance of SnO_2 thin films prepared by spray pyrolysis," *Bulletin of Materials Science*, vol. 34, no. 1, pp. 1–9, 2011.

[16] R. Lozada-Morales, O. Zelaya-Angel, and G. Torres-Delgado, "On the yellow-band emission in CdS films," *Applied Physics A*, vol. 73, no. 1, pp. 61–65, 2001.

[17] X. S. Zhao, J. Schroeder, P. D. Persans, and T. G. Bilodeau, "Resonant-Raman-scattering and photoluminescence studies in glass-composite and colloidal CdS," *Physical Review B*, vol. 43, no. 15, pp. 12580–12589, 1991.

[18] S. Lee, D. Song, D. Kin et al., "Effects of synthesis temperature on particle size/shape and photoluminescence characteristics of ZnS:Cu nanocrystals," *Materials Letters*, vol. 58, pp. 342–346, 2004.